



Title	Low-Temperature Creep at Ultra-Low Strain Rates in Pure Aluminum Studied by a Helicoid Spring Specimen Technique
Author(s)	Shen, Junjie; Yamasaki, Shigeto; Ikeda, Ken-ichi; Hata, Satoshi; Nakashima, Hideharu
Citation	MATERIALS TRANSACTIONS, 52(7), 1381-1387 https://doi.org/10.2320/matertrans.M2010405
Issue Date	2011-07-01
Doc URL	http://hdl.handle.net/2115/75556
Type	article
File Information	Low-Temperature Creep at Ultra-Low Strain Rates in Pure Aluminum Studied by a Helicoid Spring Specimen Technique.pdf



[Instructions for use](#)

Low-Temperature Creep at Ultra-Low Strain Rates in Pure Aluminum Studied by a Helicoid Spring Specimen Technique

Junjie Shen^{1,*}, Shigeto Yamasaki¹, Ken-ichi Ikeda², Satoshi Hata² and Hideharu Nakashima²

¹Department of Molecular and Materials Science, Interdisciplinary Graduate School of Engineering Sciences, Kyushu University, Kasuga 816-8580, Japan

²Department of Electrical and Materials Science, Faculty of Engineering Sciences, Kyushu University, Kasuga 816-8580, Japan

The creep behavior in pure aluminum has been investigated by helicoid spring creep tests at strain rates, $\dot{\epsilon}$, lower than 10^{-10} s^{-1} and low temperature ranging from $0.32T_m$ to $0.43T_m$. It was found that the creep behavior in this region depends strongly on grain sizes and impurity concentrations. For high-purity aluminum (5N Al) with an average grain size, $d_g > 1600 \mu\text{m}$, nearly the wire diameter of the spring sample, where the role of grain boundary during creep deformation can be negligible, the stress exponent was $n \sim 5$ and the activation energy was $Q_c = 32 \text{ kJ/mol}$. Microstructural observation showed the formation of large dislocation cells ($\sim 10 \mu\text{m}$) and tangled dislocations at the cell walls. For high-purity aluminum (5N Al) with $d_g = 24 \mu\text{m}$, the stress exponent was $n \sim 1$ and the activation energy was $Q_c = 15 \text{ kJ/mol}$. On the other hand, for commercial low-purity aluminum (2N Al) with $d_g = 25 \mu\text{m}$, the stress exponent was $n = 2$ and the activation energy was $Q_c = 25 \text{ kJ/mol}$. Microstructural observations revealed dislocations emitted from grain boundaries, those dislocations interacting with intragranular dislocations and the formation of dislocation cells in the grains. Based on those experimental results, the low-temperature creep mechanisms in pure aluminum at $\dot{\epsilon} < 10^{-10} \text{ s}^{-1}$ have been discussed. [doi:10.2320/matertrans.M2010405]

(Received November 30, 2010; Accepted April 18, 2011; Published June 1, 2011)

Keywords: pure aluminum, dislocation, ultra-low strain rate, helicoid spring creep test, grain boundary, stress exponent

1. Introduction

Creep deformation in metals and alloys follows the power-law relationship,

$$\dot{\epsilon}_s \propto \sigma^n \quad (1)$$

where $\dot{\epsilon}_s$, σ and n are steady-state strain rate, stress and stress exponent, respectively. It is known that the value of n is sensitive to deformation modes. Therefore, n is used to classify creep deformation mechanisms at different values of $\dot{\epsilon}_s$ and σ .

Up to date, deformation mechanism for $n < 3$ are not well understood even for pure metals, because such small values of n are recognized under very low strain rate, $\dot{\epsilon}$, and stress, σ , and the magnitude of n is strongly dependent on experimental conditions: temperature, T , average grain size, d_g , impurity concentration, etc. Thus, very careful experimental settings are indispensable for studying the creep with small n values, which limits reliability of creep deformation experiments conducted under very low, $\dot{\epsilon}$, and σ .

In contrast, theoretical consideration have been developed to rationalize the creep deformation at low $\dot{\epsilon}$ and σ . There are several well-known models that explain creep deformation mechanisms for small n . First, Coble diffusional creep model¹⁾ is that the flow of vacancies takes place along the grain boundaries. Second, Nabarro-Herring diffusional creep mode^{2,3)} is that the flow of vacancies takes place through the lattice. Third, Harper-Dorn type creep model⁴⁾ is related with motion of dislocations. These models with taking account of influences of d_g , T and impurity concentration have been fitted well to experimental results of creep deformation with $n < 3$ in pure aluminum at higher temperature, $T > 0.5T_m$ (T_m : melting point). However, at lower

temperature, $T < 0.5T_m$, there is still little knowledge of creep deformation with $n < 3$.

As for the creep deformation in pure aluminum at $T < 0.5T_m$, Matsunaga *et al.*⁵⁾ discovered a new creep region that shows $n = 5$ and low activation energy of $Q_c = 20\text{--}35 \text{ kJ/mol}$ under $10^{-10} \text{ s}^{-1} < \dot{\epsilon} \leq 10^{-6} \text{ s}^{-1}$. They pointed out pure metals with higher stacking fault energy (SFE) showing higher strain rates than those with lower SFE. Based on the fact, they suggested that dislocation cross-slip is a possible deformation mechanism in pure aluminum in the new creep region. After the discovery by Matsunaga *et al.*,⁵⁾ it is plausible that a creep region in pure aluminum with $n < 3$ would be found at $T < 0.5T_m$ and ultra-low $\dot{\epsilon} \leq 10^{-10} \text{ s}^{-1}$.

In order to measure creep deformation under $\dot{\epsilon} \leq 10^{-10} \text{ s}^{-1}$, a conventional uniaxial creep test needs high-resolution measurements of very small magnitudes of strain of a sample as well as very long duration of creep test, which are almost unrealistic experimental requirements. As a different approach, the helicoid spring technique can be employed. Because the helicoid spring creep test provides the highest strain sensitivity in contrast to compression and tension test.⁶⁾ A helicoid spring sample was used in the creep test for the first time by Eakin⁷⁾ and this technique was then elaborated by Burton and others.⁸⁻¹²⁾ Intensive works on low-strain rate creep using helicoid spring specimens have been done by Fiala and Čadek.^{13,14)} More recently, lots of studies on the low-strain rate creep behavior of various materials (heat-resistant steel, Ni-15%Cr solid solution alloy, pure aluminum, etc.) have been reported by L. Kloc *et al.*¹⁵⁻¹⁹⁾ Those results provided creep data that are important to analyze creep mechanisms at ultra-low $\dot{\epsilon}$, and it was revealed that extrapolation from power-law creep regime to low stress conditions can cause serious underestimation of predicted deformation rates.

*Corresponding author, E-mail: nk-j-shen@mms.kyushu-u.ac.jp

Table 1 Chemical compositions of high-purity aluminum (5N Al) and commercial pure aluminum (2N Al).

Purity	Si (ppm)	Fe (ppm)	Cu (ppm)	Mg (ppm)	Mn (ppm)	Al
5N Al	1.8	0.7	0.6	≤0.1	0.3	Bal.
Purity	Si	Fe	Cu	Mg	Mn	Al
	(mass%)	(mass%)	(mass%)	(mass%)	(mass%)	
2N Al	0.034	0.135	0.001	≤0.01	≤0.01	Bal.

In the present study, we attempt helicoids spring creep tests on pure aluminum samples to examine the possibility of a creep region with $n < 3$ at $T < 0.5T_m$. Special cares have been paid in an experimental set-up for obtaining reliable creep data under ultra-low $\dot{\epsilon}$ at an ambient temperature as well as their correct interpretations, as described below. Using the experimental apparatus using helicoid spring samples, influences of grain size and impurity concentration on the ultra-low steady-state strain rate creep deformation are examined. In order to discuss creep deformation mechanisms, microstructural observations before and after the helicoids spring creep tests are also carried out. Finally, we reach a conclusion that there is a possibility of a creep region with $n < 3$ with deformation mechanisms dependent on the grain size and impurity concentration.

2. Experimental

The experiments were performed on high-purity aluminum (5N Al) and commercial low-purity aluminum (2N Al) in the form of wires with a diameter, $d = 1.6$ mm. Chemical compositions of the specimens are shown in Table 1.

Creep tests were performed using the helicoid spring technique. There are two types of helicoid-spring creep apparatuses utilized in this study; one is for heated samples and another is for non-heated samples. Figure 1 illustrates the two apparatuses. The apparatus for heated samples in Fig. 1(a) has three adjacent heaters that are independently controlled to obtain uniform temperature distribution in the helicoids sample with an accuracy of ± 1 K. On the other hand, the apparatus for non-heated samples in Fig. 1(b) uses double insulation boxes to keep a constant sample temperature during creep tests with temperature fluctuations less than ± 1 K.

Helicoid spring specimens with a mean coil diameter, $D = 18.8$ mm, were prepared by winding the wires on threaded stainless steel bolts. The bolts with the wound wires were heat-treated to fix the helicoid shape and obtain different grain sizes. Heat treatment conditions and grain sizes after the heat treatments are shown in Table 2. After heat treatments, the helicoid spring specimen was taken off from stainless bolts very carefully using liquid lubricant to easily take off and obtain an equal interval, δ and an equal diameter, D of the coils. The helicoid specimens were cleaned using acetone in order to minimize surface effects of liquid lubricant on the creep behavior.

The following equations^{20,21)} have been employed to calculate the mean surface shear stress, τ , and the surface shear strain, γ , assuming the case of pure torsion of the helicoid spring specimen:

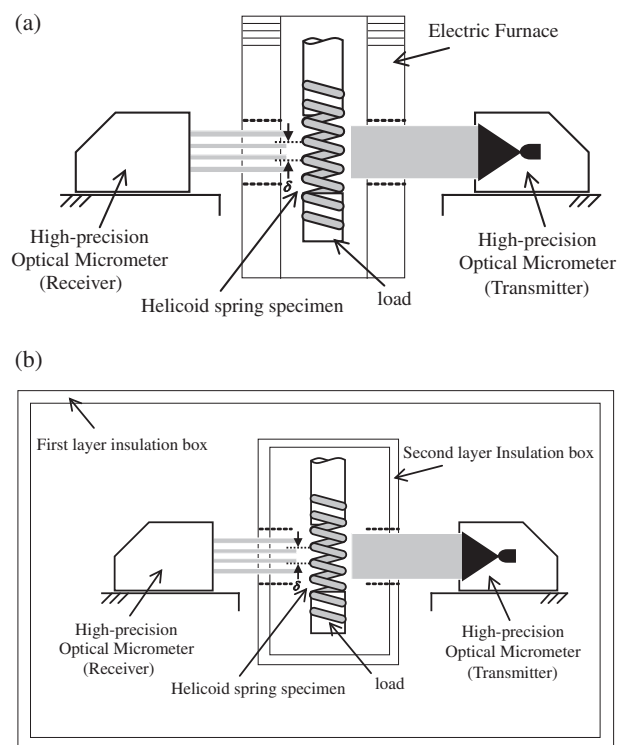


Fig. 1 The scheme of helicoid-spring creep machines. (a) Necessary to heat and (b) Unnecessary to heat (298 K).

Table 2 Heat treatment conditions and grain sizes.

Purity	Heat treatment condition	Average grain size, d_g
5N Al	Quenching from 400°C	24 μm
5N Al	Annealing at 450°C, 1 h	>1600 μm
2N Al	Annealing at 400°C, 1 h	25 μm

$$\tau = \frac{8PD}{\pi d^3}, \quad (2)$$

$$\gamma = \frac{\delta d}{\pi D^2}, \quad (3)$$

where P is the average load, D is the coil diameters, d is the wire diameters and δ is the coil pitch spacing. Since the stress and strain in the helicoids spring are essentially shear ones, they are transformed to the equivalent tensile quantities using the well-known relations: tension stress $\sigma = \sqrt{3}\tau$ and tensile strain $\epsilon = \gamma/\sqrt{3}$. In the present study, the initial coil pitch spacing is $\delta = 2.5$ mm. During creep tests, δ change from 2.5 to 3.5 mm. The data reported by Ishibashi *et al.*²²⁾ on the relation between torsion and normal elastic strains in Sn-Ag helicoid spring analyzed by the finite element method revealed that one can neglect the normal elastic strains under the condition of the coil pitch spacing between 0 to 5 mm. Therefore, the creep deformation in the present study can be considered as to be only torsion strains.

Microstructures were observed by transmission electron microscopy (TEM). TEM observation area is middle parts of cross sections of the wires. Thin foils for the TEM observation were prepared by mechanical polishing and twin-jet electropolishing using a mixture of 30% HNO_3 and 70%

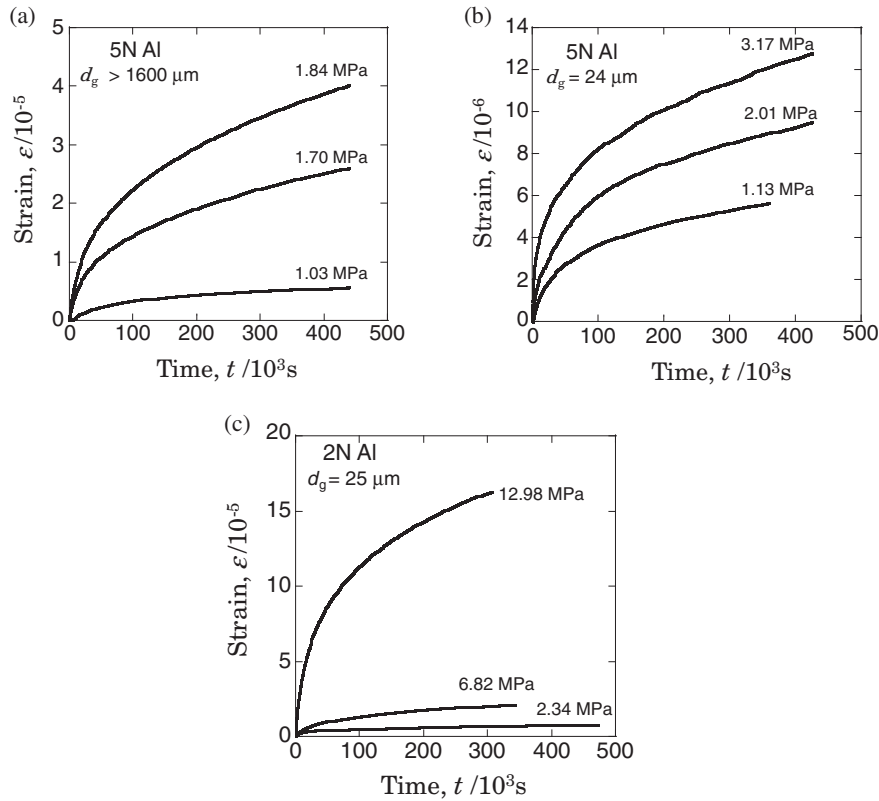


Fig. 2 Creep curves of high-purity aluminum (5 N Al) and commercial pure aluminum (2 N Al) at $0.32T_m$. (a) 5 N Al with $d_g > 1600 \mu\text{m}$ and a very small number of grains, (b) 5 N Al with average grain size, $d_g = 24 \mu\text{m}$, (c) 2 N Al with $d_g = 25 \mu\text{m}$.

methanol at 243 K. The TEM observation was conducted with a JEOL JEM-2000EX/T transmission electron microscope operated at 200 kV.

3. Results

3.1 Mechanical behavior

Examples of creep curves measured in present experiments for samples 5 N Al (a), (b) and 2 N Al (c) with different grain sizes, d_g , and different stress levels at $0.32T_m$ are shown in Fig. 2. The creep curves are characterized by pronounced primary stage, after which steady-state commenced due to work-hardening.

Figure 3 shows an example of strain rate $\dot{\epsilon}$ and temperature T plotted logarithmically against t for 5 N Al with $d_g = 24 \mu\text{m}$ at 1.13 MPa and $0.32T_m$, where the temperature was simultaneously measured during the creep test. It is apparent that the period of the temperature oscillation is approximately equal to one day (86400 s) and coincides with the period of the strain-rate oscillation. It indicates that the thermal expansion and shrinkage synchronously influence $\dot{\epsilon}$ under the conditions of ultra-low $\dot{\epsilon}$.

The Li's equation²³⁾ described below is based on the multiply and exhaustion (immobilized) of dislocations in transient creep stage. The creep curves in present study show the apparent effect of work-hardening in transient creep stage. It means that creep behavior, at least in the transient creep stage, is related with the multiply and exhaustion of dislocations. Because of that, the creep curves are fitted using the Li's equation:²³⁾

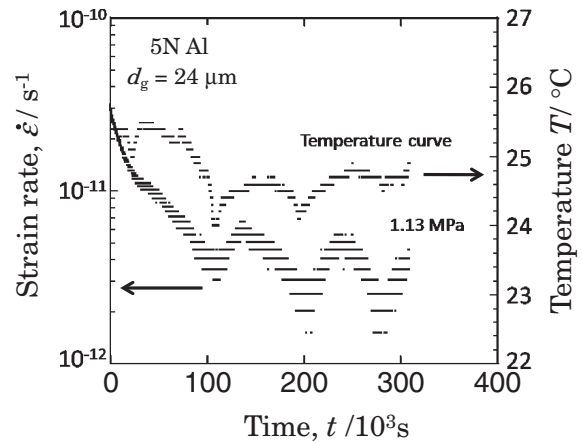


Fig. 3 Strain rate and temperature against time for high-purity aluminum (5 N Al) with $d_g = 24 \mu\text{m}$ at $0.32T_m$.

$$\epsilon = \epsilon_0 + \dot{\epsilon}_s t + \frac{\dot{\epsilon}_i}{k_1} \ln \left[1 + \frac{\dot{\epsilon}_i - \dot{\epsilon}_s}{\dot{\epsilon}_s} (1 - e^{-k_1 t}) \right] \quad (4)$$

where ϵ is the strain, ϵ_0 is the transient strain rate, $\dot{\epsilon}_s$ is the steady-state strain rate, $\dot{\epsilon}_i$ is the initial strain rate, k_1 a constant and t is the creep time.

Figure 4 shows the curve of steady-state creep rate, $\dot{\epsilon}_s$, against stress, σ . The stress exponents, n , are calculated from straight slopes. For sample 5 N Al, the stress exponent is $n \sim 5$ for $d_g > 1600 \mu\text{m}$, while $n \sim 1$ for $d_g = 24 \mu\text{m}$. For sample 2 N Al, the stress exponent is $n = 2$ for $d_g = 25 \mu\text{m}$. These facts indicate that creep behavior at low temperature

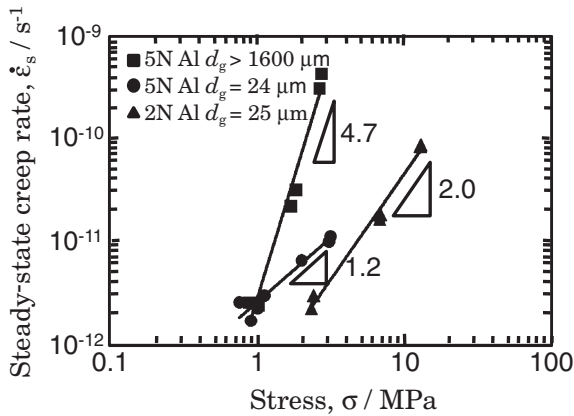


Fig. 4 Steady-state creep rate against stress in double logarithm coordinates for high-purity aluminum (5N Al) and commercial pure aluminum (2N Al) at $0.32T_m$.

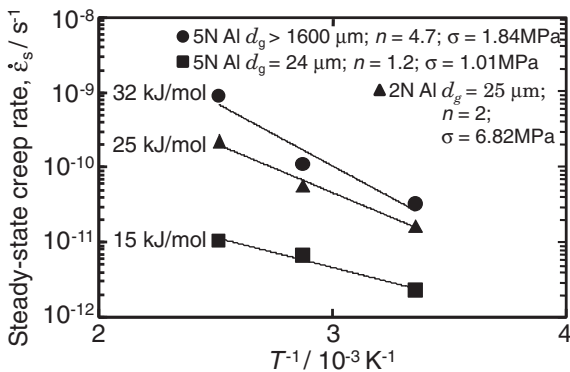


Fig. 5 Temperature dependence on the steady-state creep rate. The activation energy is $Q = 32$ kJ/mol for sample 5N Al with $d_g > 1600$ μm and a very small number of grains, $Q = 15$ kJ/mol for sample 5N Al with $d_g = 24$ μm and $Q = 25$ kJ/mol for sample 2N Al with $d_g = 25$ μm .

and ultra-low strain rates depends on the grain sizes as well as impurity concentrations.

Figure 5 shows $\dot{\epsilon}_s$ in logarithmic scale plotted against the reciprocal temperature, $1/T$. The relation of the activation energy, Q_c , is calculated by Arrhenius equation;

$$\dot{\epsilon}_s = A \exp\left(-\frac{Q_c}{RT}\right) \quad (5)$$

where A is a constant depended on materials and stress, R is the gas constant, T is the absolute temperature. The activation energy is $Q_c = 32$ kJ/mol for sample 5N Al with $d_g > 1600$ μm , while $Q_c = 15$ kJ/mol for $d_g = 24$ μm . For sample 2N Al with $d_g = 25$ μm , the activation energy is $Q_c = 25$ kJ/mol.

3.2 Microstructural characters

The microstructural observation was motivated by the fact that all the creep curves in Fig. 3 showed the effect of work hardening. It means that all of the creep deformation at the different stress exponents is correlated with motions of dislocations. Thus, the objective of the microstructure observation was to certify whether the creep behavior is

related to the motions of dislocations and what kinds of dislocation motions are correlated.

A comparison on microstructure of pure aluminum specimens after creep tests with the initial state before creep tests is showed in Fig. 6. Low density of dislocations in sample 5N Al with $d_g > 1600$ μm and 2N Al with $d_g = 25$ μm after annealing is proved by two-beam excitation imaging conditions, $\vec{g} = 0\bar{2}2$ (a) and $\vec{g} = 0\bar{2}0$ (c). Figure 6(b) shows higher dislocation density and formation of dislocation cells after quenching. After creep tests, dislocation cells composed by tangled dislocations in cell boundaries are formed with an average cell diameter of 10 μm in sample 5N Al with $d_g > 1600$ μm (d) and 3 μm in 2N Al with $d_g = 25$ μm (f). The dislocation cells in sample 2N Al are formed surrounding particles indicated by the arrow. No remarkable difference in dislocation density, dislocation-cell sizes and dislocation arrangements between the crept (b) and non-crept samples (e) is observed.

Figure 7 shows dislocation structure near to grain boundaries in sample 2N Al with $d_g = 25$ μm crept at 2.34 MPa and $0.32T_m$ with the stress exponent, $n = 2$. Figure 7(a) indicates the dislocations emission and multiplication from a grain boundary between particles like a ‘‘Frank-Read source’’. The arc-shaped dislocations are pinned by particles and induced to arc. Figure 7(b) show dislocation emission from a grain boundary in a way of ‘‘random distribution’’ where there are no particles. The emitted dislocations interact with intragranular dislocations. A Burgers vector analysis revealed that those dislocations are normal dislocations with $\vec{b} = \frac{a}{2} [1\bar{1}0]$ (a: lattice parameter), which indicates that emitted dislocations from grain boundaries have the character of intragranular dislocations on $\{1\bar{1}1\}$ slip planes.

4. Discussion

Figure 8 summarizes the present creep data obtained by the present helicoid spring creep tests and the data reported by Matsunaga *et al.*⁵⁾ by uniaxial creep tests for high-purity aluminum at room temperature ($0.32T_m$). The present investigation revealed a low stress creep deformation region of $n < 3$, region I. Creep behavior of sample 5N Al at ultra-low strain rates, $\dot{\epsilon} < 10^{-10}$ s^{-1} , with $d_g = 24$ μm in region I shows smooth connection to the low temperature, low activation energy dislocation creep in region II.⁵⁾ The transition stress, σ , from range I to II indicated by the arrow with a dashed line, is comparable with $\sigma_{0.2}$ (0.2% proof stress) that corresponds to a resolved shear stress (τ_{RSS}) of 7 MPa for 5N Al with $d_g = 140$ μm .⁵⁾ The present research shows three types of creep behavior in region I that tightly depending on grain sizes and impurity concentrations.

4.1 The effect of grain sizes

For high-purity aluminum (5N Al) with $d_g = 24$ μm , a stress exponent is $n \sim 1$ and the activation energy is $Q_1 = 15$ kJ/mol. The mechanisms of creep generally associated with $n = 1$ are Coble creep, Harper-Dorn creep and Nabarro-Herring creep. However, these mechanisms require higher activation energy (lattice diffusion energy, $Q_L \sim 142$ kJ/mol, or grain boundary diffusion energy, $Q_{gb} \sim 85.2$ kJ/mol, for pure aluminum) than the value in this study.

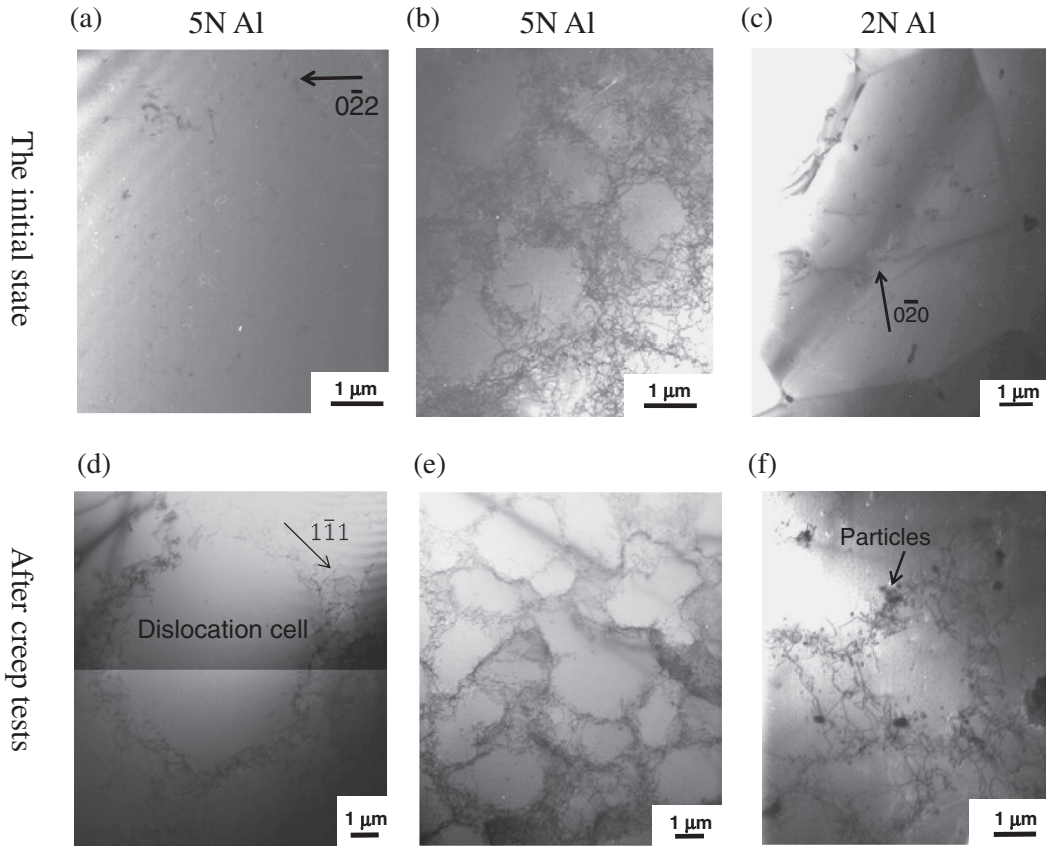


Fig. 6 Comparison on microstructure of pure aluminum samples after creep tests with the initial state before creep tests. (a), (b) and (c) are dislocation substructures in initial specimens and (d), (e) and (f) are dislocation substructure in crept specimens. (a) after annealing: 450°C, 1 h and (d) crept at $\sigma = 2.67$ MPa and $\epsilon = 2.74 \times 10^{-4}$ in sample 5 N Al with $d_g > 1600 \mu\text{m}$, (b) after quenching from 400°C and (e) crept at $\sigma = 0.91$ MP and $\epsilon = 4.76 \times 10^{-6}$ in sample 5 N Al with $d_g = 24 \mu\text{m}$, (c) after annealing: 400°C, 1 h and (f) crept at $\sigma = 2.34$ MPa and $\epsilon = 5.04 \times 10^{-6}$ in sample 2 N Al with $d_g = 25 \mu\text{m}$.

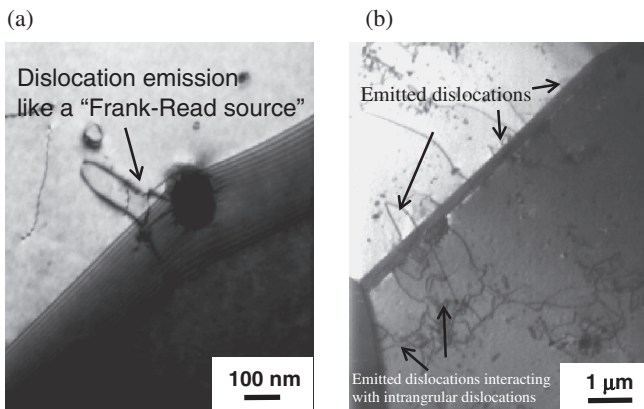


Fig. 7 Dislocation structure in sample 2 N Al with $d_g = 25 \mu\text{m}$ crept at $\sigma = 2.34$ MPa, $\epsilon = 5.04 \times 10^{-6}$ and $T = 0.32T_m$. (a) lattice dislocations emission from a grain boundary like a Frank-Read source (b) lattice dislocations emission from a grain boundary and emitted dislocations interacting with intragranular dislocations.

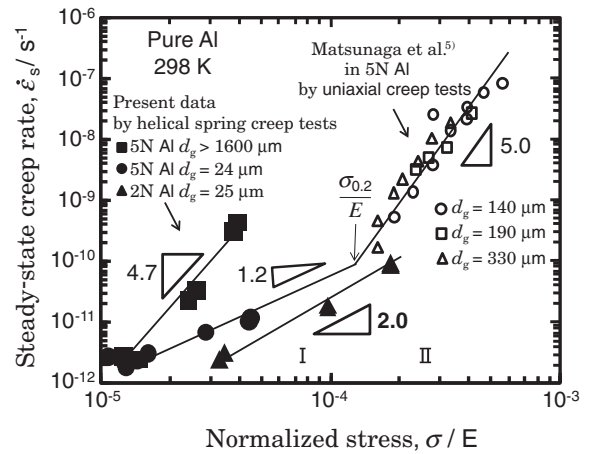


Fig. 8 A summary of steady-state creep rate against stress normalized by elastic modulus for pure aluminum measured in the present study by helical spring creep tests and earlier investigations for 5 N Al by uniaxial creep tests at $0.32T_m$.

Furthermore, the change of dislocation arrangement generally expected in the case of deformation controlled Harper-Dorn creep has not been observed. Thus those creep mechanisms can be ruled out as possible rate-controlling mechanism. Another creep mechanism associated with $n = 1$ is intrinsic grain boundary sliding (IGBS). The IGBS is that

the grain boundary sliding is not inhibited by the secondary phases, particles, grain boundary intersections or grain boundary ledges, and has been described by Arzt and Ashby.²⁴⁾ In that case, grain boundary sliding exhibit the Newton viscous behavior ($n = 1$). The mechanism of IGBS is still not enough clear, and generally thinking, it is climb of

grain boundary dislocations.²⁵⁾ Thus, the activation energy for IGBS is equal to grain boundary diffusion Q_{gb} and around $0.5\text{--}0.8 Q_L$. In this study, the activation energy Q_1 is around $0.43\text{--}0.75 Q_2$. The value of Q_2 is $20\text{--}35 \text{ kJ/mol}$,⁵⁾ and according to motion (cross-slip) of intragranular dislocations. As a nature considering, the creep with Q_1 should occur in the grain boundary. Therefore, the creep mechanism may be associated with IGBS. However, the mechanism of IGBS in this study can not be described by climb of grain boundary dislocations due to lower activation energy. Thus, the creep mechanism is suggested as “low- T and low- Q IGBS”.

However, for sample 5 N Al with $d_g > 1600 \mu\text{m}$, where the contribution of grain boundaries to creep deformation can be negligible due to the large d_g , the stress exponent was $n \sim 5$ and the activation energy is $Q_2 = 32 \text{ kJ/mol}$. The microstructural characteristics showed the formation of large dislocation cells and tangled dislocations at cell boundaries that are different from the dislocation substructure in the steady-state creep region at high temperatures and high strain rate which are characterized as subgrains and Frank networks within subgrain boundaries.²⁶⁾ On the other hand, the dislocation substructure observed in sample 5 N Al with $d_g > 1600 \mu\text{m}$ tends to be similar to the dislocation cell structure¹²⁾ in high purity aluminum (5 N Al) crept at low temperature. However, the average dislocation-cell size, $10 \mu\text{m}$, in our investigation is larger than that $1 \mu\text{m}$ observed by Matsunaga *et al.*⁵⁾ The large dislocation cells provide less shear stress activating Frank-Read sources in Al, as shown in the following eq. (6).

Frank-Read sources in Al can generate dislocations inside a dislocation cell, which is expressed as the equation:

$$\tau_{F.R.} = \mu b / \lambda, \quad (6)$$

where $\tau_{F.R.}$ is the shear stress activating the Frank-Read source, μ is the shear modulus of 25.4 GPa in pure Al, b is the magnitude of Burgers vector of $2.86 \times 10^{-10} \text{ m}$, λ is dislocation cell size. In the present investigation, $\lambda \sim 10 \mu\text{m}$. Thus, $\tau_{F.R.}$ is evaluated to be about 0.7 MPa that is less than the minimum shear stress, 0.89 MPa in the present investigation. Therefore, we suggest that creep occurs through the supply of dislocations inside dislocation cells under stresses greater than $\tau_{F.R.}$.

4.2 Effect of impurity concentration

For the commercial low-purity aluminum (2 N Al), the stress exponent is $n = 2$. Microstructural observation showed the dislocation emission from grain boundaries, those dislocations interacting with intragranular dislocations and the formation of dislocation cells in the grains. The emission of dislocations from grain boundaries is similar to that from the generally “Frank-Read source”. That is, we can assume that dislocations can be emitted from “weak areas” of grain boundaries having lower energy. Here, “Weak areas” of grain boundaries are those regions of misfit in grain boundaries (Mott, 1948). The dislocation emission from grain boundary provides a direct evidence of grain boundary sliding in Fig. 7(a) and (b). The formation of intragranular dislocation cells means that grain-interior deformation also contributes to total deformation. In those cases, the creep can be considered as extrinsic grain boundary sliding (EGBS)

elaborated by Crossman and Ashby.²⁷⁾ The EGBS is that the grain boundary sliding is inhibited by the secondary phase, particles, grain boundary intersection and grain boundary ledge, and grain boundary sliding must be accommodated by grain-interior deformation. However, The EGBS in this study is different with generally EGBS because the activation energy is $Q_3 = 25 \text{ kJ/mol}$ that can compare with the value, $Q_3 = 32 \text{ kJ/mol}$ at $n \sim 5$ for 5 N Al. Thus, the low- T and low- Q EGBS can be considered to be controlled by cross-slip of emitted dislocations from grain boundary. The microstructural characters, the formation of lattice dislocation cells in the grains, in sample 2 N Al are similar to that in sample 5 N Al at stress exponent, $n \sim 5$. The average dislocation-cell size, $\sim 3 \mu\text{m}$, is smaller than $\sim 10 \mu\text{m}$ observed in 5 N Al at stress exponent, $n \sim 5$. The shear stress, $\tau_{F.R.}$ calculated from the eq. (6) is about 2.3 MPa that is approximately equal to the minimum shear stress, 2.34 MPa in the present investigation. It means that the applied stresses in the present investigation are able to activate the Frank-Read sources in the dislocation cells.

It is therefore suggested that there are three kinds of creep behavior depending on grain sizes and impurity concentrations at $T < 0.4T_m$ and $\dot{\epsilon} < 10^{-10} \text{ s}^{-1}$. The creep behaviors are controlled by low- T and low- Q intrinsic grain boundary sliding in high-purity aluminum (5 N Al) with $d_g = 24 \mu\text{m}$; low- T and low- Q extrinsic grain boundary in low-purity aluminum (2 N Al) with $d_g = 25 \mu\text{m}$; low- T and low- Q dislocation creep in 5 N Al with $d_g > 1600 \mu\text{m}$. The detailed rate-controlled creep mechanisms in this region are still unclear and need further research.

5. Conclusions

Creep behavior and microstructural characters of high-purity aluminum (5 N Al) and commercial low-purity aluminum (2 N Al) with different grain sizes have been investigated at $T < 0.4T_m$ and $\dot{\epsilon} < 10^{-10} \text{ s}^{-1}$. The present investigation shows three kinds of creep behavior strongly depending on grain sizes and impurity concentrations:

- (1) For high-purity aluminum (5 N Al) with an average grain size is $d_g > 1600 \mu\text{m}$ nearly the wire diameter of the spring sample, where the role of grain boundary during creep deformation can be negligible, where the stress exponent was $n \sim 5$ and the activation energy was $Q = 32 \text{ kJ/mol}$. Microstructural observation shows the formation of large cell ($\sim 10 \mu\text{m}$) and tangled dislocations at the cell walls. The creep deformation is consistent with low- T and low- Q dislocation creep. Because the applied stress is enough to activate the Frank-Read sources in the dislocation cells, the creep is considered occurring through the supply of dislocations inside dislocation cells creep.
- (2) For high-purity aluminum (5 N Al) with $d_g = 24 \mu\text{m}$, the stress exponent was $n \sim 1$ and the activation energy was $Q = 15 \text{ kJ/mol}$. No apparent change of microstructure has been observed. The creep deformation is suggested as low- T and low- Q intrinsic grain boundary sliding (IGBS).
- (3) For commercial low-purity aluminum (2 N Al) with $d_g = 25 \mu\text{m}$, the stress exponent was $n = 2$ the activa-

tion energy was $Q = 25$ kJ/mol. Microstructural observations revealed dislocation emission from grain boundary, those dislocations interacting with intragranular dislocations and the formation of dislocation cells in the grains. The creep deformation is suggested as low- T and low- Q extrinsic grain boundary sliding (EGBS).

Acknowledgements

This work was supported in part by the Grants-in-Aid from the Japan Society for the Promotion of Science (JSPS) and the Grants-in-Aid from the Ministry of Education, Culture, Sports, Science and Technology (MEXT), Japan.

REFERENCES

- 1) R. L. Coble: *J. Appl. Phys.* **34** (1963) 1679–1682.
- 2) F. R. N. Nabarro: *Rept. Conf. on the solids*, (The Physical Society, London, 1948) p. 78.
- 3) C. Herring: *J. Appl. Phys.* **21** (1950) 437–445.
- 4) J. Harper and J. E. Dorn: *Acta Metall.* **5** (1957) 654–665.
- 5) T. Matsunaga, S. Ueda and E. Sato: *Scr. Mater.* **63** (2010) 516–519.
- 6) L. Kloc and P. Mareček: *J. Test. Evaluation* **37** (2009) 53–58.
- 7) C. T. Eakin: *Prod. Eng. (N.Y.)* **27** (1956) 186–190.
- 8) B. Burton and G. W. Greenwood: *Met. Sci. J.* **4** (1970) 215–218.
- 9) B. Burton and G. L. Reynold: *Acta Metall.* **21** (1973) 1073–1078.
- 10) I. G. Crossland, R. B. Jones and G. W. Lewthwaite: *J. Physic D* **6** (1973) 1040–1046.
- 11) D. J. Towle and H. Jones: *Acta Metall.* **24** (1976) 399–407.
- 12) B. Burton: *Acta Metall.* **26** (1978) 1237–1241.
- 13) J. Fiala, J. Novotný and J. Čadek: *Mater. Sci. Eng.* **60** (1983) 195–206.
- 14) J. Novotný, J. Fiala and J. Čadek: *Acta Metall.* **33** (1985) 905–911.
- 15) L. Kloc, J. Fiala and J. Čadek: *Mater. Sci. Eng. A* **130** (1990) 165–172.
- 16) L. Kloc, J. Fiala and J. Čadek: *Mater. Sci. Eng. A* **202** (1995) 11–17.
- 17) L. Kloc and V. Sklenička: *Mater. Sci. Eng. A* **234** (1997) 962–965.
- 18) L. Kloc, V. Sklenička and J. Ventruba: *Mater. Sci. Eng. A* **319** (2001) 774–778.
- 19) L. Kloc and V. Sklenička: *Mater. Sci. Eng. A* **387** (2004) 633–638.
- 20) S. Timoshenko and D. H. Yong: *Elements of Strength of Materials*, fifth edition, (Van Nostrand, New York, 1968) pp. 77–80.
- 21) A. M. Wahli: *Mechanical Springs*, second edition, (McGraw-Hill, New York, 1963) pp. 229–230.
- 22) M. Ishibashi, K. Fujimoto, K. Ikeda, S. Hata and H. Nakashima: *J. Japan Inst. Metals* **73** (2009) 373–380.
- 23) J. C. M. Li: *Acta Metall.* **11** (1963) 1269–1270.
- 24) E. Arzt, M. F. Ashby and R. A. Verrall: *Acta Metall.* **31** (1983) 1977–1989.
- 25) R. S. Gates: *Acta Metall.* **21** (1973) 855–864.
- 26) D. Caillard and J. L. Martin: *Acta Metall.* **30** (1982) 437–445.
- 27) F. W. Crossman and M. F. Ashby: *Acta Metall.* **23** (1975) 425–440.